ACS ES&T Air

pubs.acs.org/estair

Article

Multimodal Approach for Assessing Emissions and Transport of Greenhouse Gases and Air Pollutants from the January 2025 Los Angeles Wildfires

Published as part of ACS ES&T Air special issue "The 2025 Los Angeles Fires".

Pietro F. Vannucci,* Wenye Wang, Jooil Kim, Timothy Lueker, and William M. Berelson

Cite This: https://doi.org/10.1021/acsestair.5c00430

Read Online

ACCESS | Metrics & More | Article Recommendations | Supporting Information

Downloaded via William Berelson on February 21, 2026 at 21:01:24 (UTC).
See https://pubs.acs.org/sharingguidelines for options on how to legitimately share published articles.

ABSTRACT: Wildfires are an increasingly dominant source of greenhouse gases and criteria air pollutants in urbanized regions. Continuing to refine quantifications of the atmospheric impacts of urban wildfires is an important goal to improve predictions of future events relevant to both the global carbon budget and public exposure. Here, we analyze the January 2025 Los Angeles (LA) wildfires by integrating satellite imaging, meteorological models, advection and diffusion models, and dense ground-level air quality observations from both low-cost sensors and reference-grade instruments. Focusing specifically on the Eaton fire, we demonstrate how its emissions were transported across LA, noting the rate of spread and the magnitude of pollutant enhancements achieved. We complement our measurements with bottom-up estimates of the carbon content lost from the fires and corroborate our approach through a Gaussian dispersion plume analysis. Our analyses indicate that the Eaton fire consisted of two distinct periods of burning which differentially consumed structures and vegetation, and our bottom-up budget and atmospheric observations agree that the combustion of structures released significantly more carbon than that of vegetation. During the period of most intense burning, emission rates of CO (CO_2) were estimated to be approximately 21.2−37.6× (0.9−1.2×) greater than average daily anthropogenic contributions. Subsequent observational evidence of pollutant concentrations also highlights the outsized contribution of wildfire CO emissions, relative to normal conditions. The impact of wildfire emissions on fine particulate matter is then assessed through the lens of both primary emissions and potential secondary formation. Additionally, we note how spikes in methane concentrations point to wildfire-driven destruction of natural gas infrastructure. Together, these results demonstrate the value of our multimodal approach in elucidating a holistic picture of the consequences of urban wildfires with respect to public health and greenhouse gas emissions.

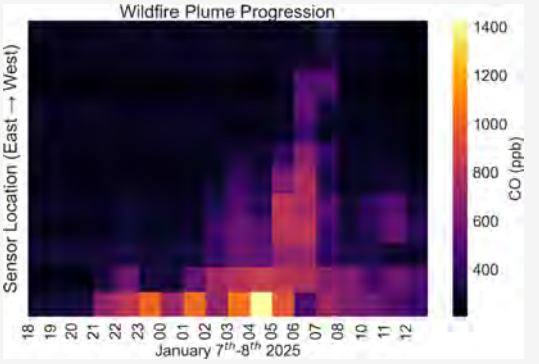

KEYWORDS: *urban wildfires, low-cost sensor networks, carbon budget, satellite remote sensing, Gaussian plume dispersion*

INTRODUCTION

Large-scale climatic changes are leading to an increase in the incidence and intensity of wildfires across many regions of our planet, and especially at the wildland−urban interface (WUI) in regions that are drying.[1−4] This development is environmentally problematic both with regards to exacerbating climate change (through increased emissions of greenhouse gases (GHGs) such as carbon dioxide (CO_2) and methane (CH_4)) and degrading air quality (through increased emissions of criteria air pollutants such as carbon monoxide (CO) and fine aerosols of a diameter smaller than 2.5 μm ($PM_{2.5}$)). There is also the direct loss of vegetation that acts as a sink for CO_2 and air pollutants alike. Moreover, when wildfire emissions occur near (and/or are transported) to urban centers, they can constitute severe public health burdens. This consideration is compounded by the fact that urban wildfires often combust a wide range of materials beyond biomass, and the impact of these varied combustion products on human exposure is an active area of research.[5]

The relevance of wildfire smoke as a threat to public health will only continue to grow, especially in the United States, where the number of homes at the WUI is rising rapidly[6] and nonwildfire sources of air pollutants are on the decline.[7,8] Therefore, quantifying the magnitude of wildfire emissions of both GHGs and air pollutants and determining how these emissions spread though urban environments and impact

Received: October 28, 2025
Revised: February 11, 2026
Accepted: February 12, 2026

ACS Publications © XXXX American Chemical Society

human exposure is an important contribution toward improving our risk assessments of future wildfires. Here, we examine the January 2025 Southern California wildfires, a series of fires impacting two regions within the Los Angeles metro area and ultimately resulting in the destruction of nearly 60,000 acres of land and more than 15,000 structures.[9] The largest conflagrations were the Palisades and Eaton fires. We focus on the Eaton fire specifically, because its location relative to the dominant winds during this period resulted in its smoke affecting Los Angeles citizens most immediately and directly (whereas smoke from the Palisades fire was largely transported offshore upon emission). Our goal in this study is to integrate satellite imaging, meteorological models, and ground-based, high-spatial density air quality observations to assess the Eaton fire in terms of the extent of the destruction of vegetation and structures, the magnitude of the resulting emissions of criteria air pollutants and greenhouse gases, and the transport and impact of these emissions on local air quality.

We utilize satellite imaging to track the development of the wildfires and to quantify how their intensity varied over time. Doing so, we are able to independently establish a timeline of the fires' progression and better elucidate the connection between periods of burning and the subsequent atmospheric impacts. We also employ satellite outputs and aerial photography to evaluate the total area of trees, shrubs, and structures lost. From this, we seek to estimate the amount of carbon released by the fires to understand how these emissions compare to typical anthropogenic contributions.

Meteorology played a key role in the inception of the fires and the subsequent spread of emissions. An extended dry period accompanied by exceptionally strong Santa Ana winds created the conditions necessary for these devastating fires to break out and spread in a remarkably quick manner.[10] These same conditions, however, also played a part in mitigating the abundance of pollutants by virtue of their rapid transport offshore, thus lessening public exposure to the toxic criteria air pollutants emitted by the fires. We therefore probe meteorological models to understand how the wind speed, wind direction, and boundary layer height (BLH) evolved as the fires progressed.

To evaluate the atmospheric impacts of these fires, we make use of two independent air quality networks situated within a greater LA area. The first is the Berkeley Environmental Air-quality and CO_2 Network (BEACO$_2$N, https://beacon.berkeley.edu/about/). Originally deployed in the San Francisco Bay Area, it has since expanded to multiple cities around the United States, Europe, and Oceania, seeking to provide high temporal and spatial density measurements of CO_2, CO, nitrogen monoxide (NO), nitrogen dioxide (NO_2), ozone (O_3), and $PM_{2.5}$ utilizing economically advantageous sensors. Several studies have previously described the design and capabilities of this network in great detail.[11−17] The Los Angeles BEACO$_2$N subnetwork is managed by researchers at the University of Southern California (USC), and we refer to it as the Carbon Census (CC) network. We complement observations from the CC network with data from the Los Angeles Megacity Carbon Project (LAMC, https://www.nist.gov/programs-projects/los-angeles-megacity-carbon-project), a network managed by the National Institute of Standards and Technology (NIST) measuring CO, CO_2, and CH_4 across Southern California.[18,19] LAMC measurements provide a valuable comparison by offering insights on atmospheric trends both upwind and downwind of the CC network and in even closer proximity to the outbreaks of the Palisades and Eaton fires. We note the presence of long-standing regulatory-grade measurement sites in the city of Los Angeles, such as those managed by the Environmental Protection Agency Air Quality System (EPA AQS) and the South Coast Air Quality Management District (SCAQMD). However, we do not make use of data from this network as it does not provide insights on CO_2, which is an integral part of our analysis. Additionally, we find some overlap in the regions of the city covered by EPA AQS and LAMC sites, such as in Pasadena (AQS ID: 06-037-2005) and downtown Los Angeles (AQS ID: 06-037-1103).

Through this unified approach, we aim to provide a clear picture of how these wildfires uniquely impacted LA air quality. We demonstrate the value of this high spatial density low-cost air quality sensor network, the potential for enhancing our observations through the aggregation of auxiliary datasets, and the use of plume dispersion models to help relate transport to observed concentrations at the urban scale.

METHODOLOGY AND DATASET CURATION

The January 2025 Southern California wildfires began on January 7th, 2025 and were not officially declared contained until January 31st. We thus delineate our study period as January 1st−31st, covering the entirety of the fires plus the week prior to establish a baseline for comparison. However, because the bulk of the destruction occurred in the days immediately following the outbreak, we dedicate particular attention to this initial period.

Satellite Imagery

We take advantage of National Aeronautics and Space Administration (NASA) and National Oceanic and Atmospheric Administration (NOAA) assets to acquire satellite imagery, namely from the NOAA Geostationary Operational Environmental Satellite 18 (NOAA GOES-18). We follow the temporal development of the wildfires in daytime conditions through images captured by the blue, red, and near-infrared bands, which allow us to track the emanation and spread of smoke plumes. We also utilize shortwave infrared radiation (SWIR) band images to assess nighttime conditions. SWIR is a proxy for thermal enhancements, and the intensity of this band correlates with temperature anomalies caused by fire activity.[20] As such, we are able to track the fires not only at all hours of the day but also in spite of the presence of clouds which may obscure the detection of smoke plumes. Moreover, analyzing SWIR lets us quantify the relative magnitude of fires across the burn period, as shortwave infrared radiation correlates with combustion intensity.

Supporting Information (SI) Figure S1 demonstrates how smoke from the Palisades fire was largely carried off-shore and therefore did not greatly influence the city of LA, at least not in the first 24 h. On the other hand, on account of the prevailing northeasterly winds, emissions from the Eaton fire traveled directly across the high-population-density urban core. Therefore, we are particularly interested in quantifying the total biomass and combustion material destroyed here (considering trees, shrubs, and structures) in order to estimate the total amount of carbon released from these fires.

To track the loss of vegetation, we utilize European Space Agency (ESA) Sentinel-2 satellite imagery to evaluate changes in the Normalized Difference Vegetation Index (NDVI) over the affected area before and after the fire. Training a model to distinguish shrubs (defined as less than 4 m tall) from trees, we

https://doi.org/10.1021/acsestair.5c00430
ACS EST Air XXXX, XXX, XXX−XXX

Table 1. CC Network Metadata[a]

Node ID #	Node Location Name	Latitude	Longitude	Elevation (m)	CO	CO_2	$PM_{2.5}$
206	USC	34.02	-118.287	91	✓	✓	✓
207	Castelar	34.064	-118.24	113	-	✓	-
208	Pio Pico	34.045	-118.317	73	✓	-	✓
209	Wilshire	34.058	-118.343	65	✓	✓	✓
211	10th Street	34.047	-118.273	84	✓	✓	✓
213	Dorsey	34.023	-118.348	47	✓	✓	✓
215	Foshay	34.019	-118.306	67	✓	✓	✓
216	9th Street	34.036	-118.247	86	✓	✓	-
217	Murchison	34.06	-118.196	131	✓	✓	✓
220	3rd Street	34.07	-118.335	80	✓	-	✓
292	Nora Sterry	34.044	-118.447	84	-	✓	✓
294	HOLA	34.063	-118.283	101	-	✓	✓
305	LACES	34.045	-118.372	41	-	✓	✓
306	Venice High	33.997	-118.445	25	✓	✓	✓
308	Mar Vista	34.016	-118.435	46	✓	✓	✓
309	Manual Arts	34.009	-118.292	65	✓	✓	✓

[a]Node locations refer to the locations where CC nodes are installed. Green check marks indicate the presence of corrected observations of each pollutant for the study period. Note: Elevation represents the height at which the measurement is taken, combining distance above ground and above sea level.

Table 2. LAMC Network Metadata[a]

Site ID	Full Name	Latitude	Longitude	Elevation (m)	CO	CO_2	CH_4
CIT	Caltech	34.137	-118.126	278	✓	✓	✓
USC	University of So. Cal.	34.021	-118.289	105	-	✓	✓
RAN	Santa Monica	34.0095	-118.491	41	✓	✓	✓

[a]. Boxes filled with checks indicate the presence of corrected observations of each pollutant for the study period. Note: Elevation represents the height at which the measurement is taken, combining distance above ground and above sea level.

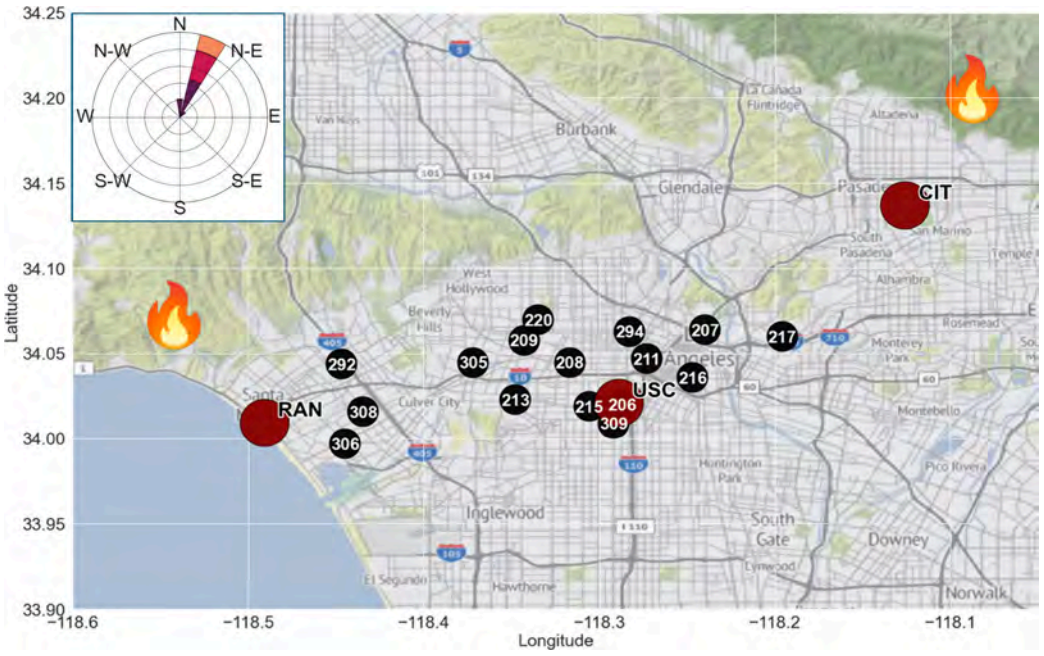

Figure 1. Partial map of the greater LA area showing CC (black) and LAMC (maroon) node locations, also with respect to where the Palisades (left) and Eaton (right) fires broke out. Note the colocation of CC node 206 and LAMC site USC. The wind rose then denotes the average wind direction at the CIT site between January 7th and 8th.

assess the total area of shrub and tree canopy burned. To estimate the area of structures lost, we utilize high-resolution Google Earth images and cross-reference building boundaries from the Los Angeles Region Imagery Acquisition Consortium (LARIAC, https://lariac-lacounty.hub.arcgis.com/). The specific methods and assumptions we employ to convert these areas to quantities of carbon released are described in detail in our Supporting Information.

https://doi.org/10.1021/acsestair.5c00430
ACS EST Air XXXX, XXX, XXX−XXX

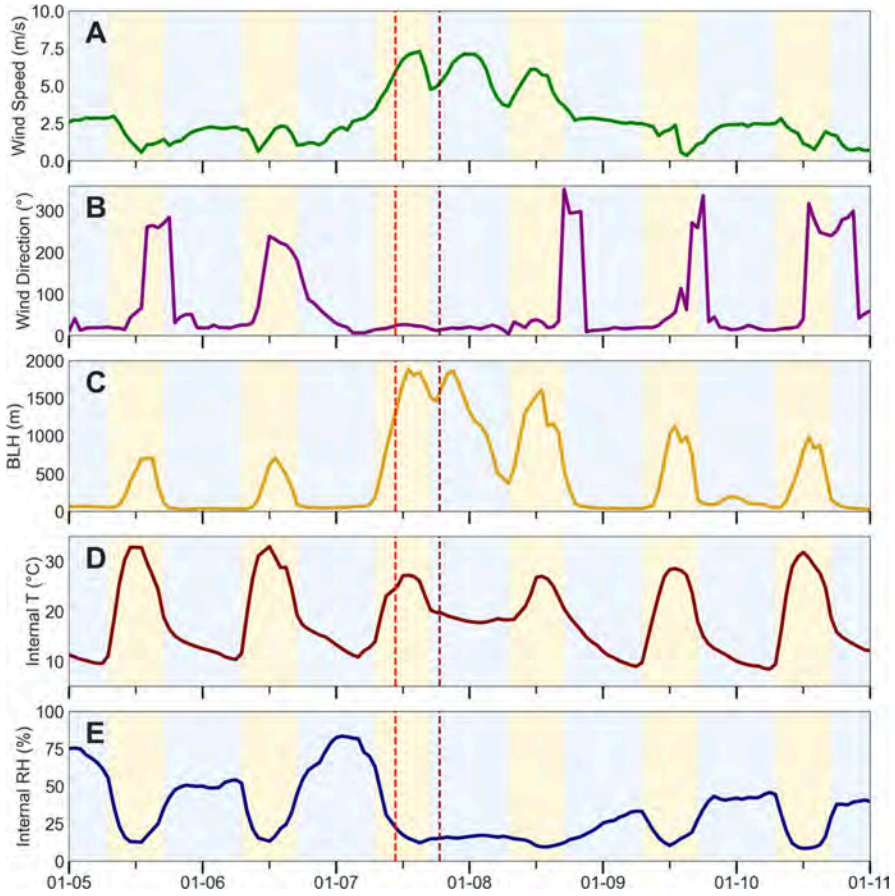

Figure 2. Meteorological parameters of interest during the onset of the fires: (A) wind speed, (B) wind direction, (C) boundary layer height, (D) temperature, and (E) relative humidity. Panels A−C are constructed from ERA5 model outputs. Panels D and E then represent the average of internal measurements taken within CC sensor boxes. Yellow shading represents daytime hours, and blue shading represents nighttime hours. The red and maroon dashed lines then represent the time of outbreak of the Palisades and Eaton fires, respectively.

Meteorology

The fires started and spread, in large part, due to the unusually strong Santa Ana wind conditions, which drive air from the NNE across the San Gabriel mountains and through Los Angeles. We assess meteorological conditions across the study period by employing the European Centre for Medium-Range Weather Forecasts Reanalysis v5 (ERA5) model.[21] We query hourly estimates of BLH and latitudinal/longitudinal wind speeds and directions at 10 m above ground for the month of January 2025. The spatial bounds are chosen as (33, 35) for latitude and (−119, −117) for longitude at a resolution of 0.25°×0.25°. We subsequently pair these meteorological estimates to our air quality measurements by matching sensor locations to the nearest model grid cell(s) at each hourly time step. Finally, we confirm the accuracy of these model estimates through comparison with wind speed observations taken at a weather station at Whittier Hills (33.984, −118.010),[22] about 25 km from the fire origin (Figure S2). In the following sections, we explore how the CC and LAMC networks allowed us to track the dispersion of emissions from the January 2025 LA wildfires through the lens of these unique meteorological conditions.

Air Quality Observations

Table 1 lists the CC nodes active at the time of the wildfires, their locations, and calibrated pollutant measurements available at each node. The calibration methods we utilize to establish pollutant concentrations are outlined in previous studies: Delaria et al.[12] focus on CO_2, Patel et al.[14] on $PM_{2.5}$, and Winter et al.[16] on $CO/O_3/NO/NO_2$. On account of reference-grade observation availability for calibration, this study is able to present corrected CC records of CO, CO_2, and $PM_{2.5}$ for January 2025. In terms of instrumentation, CC nodes utilize Vaisala GMP343s for measuring CO_2, Alphasense CO-B 4s for CO, and Plantower PMS5003s for $PM_{2.5}$.

Analogous to Table 1, Table 2 lists the relevant LAMC sites we consider in this study and the pollutant measurements available at each. Of the 12 total sites operated by the LAMC network, we make use of three: "CIT", located at the California Institute of Technology in Pasadena, near the location of the Eaton fire; "USC", located in downtown LA at the University of Southern California, colocated with CC node 206; and "RAN", in Santa Monica, located at the westernmost end of our CC array. The calibration methods utilized to correct these observations are outlined in previous studies.[18,19] In terms of instrumentation, LAMC sites use Picarro G2301s and G2401s to measure CO, CO_2, and CH_4. We depict the locations of both CC and LAMC measurement points graphically in Figure 1. In understanding pollutant transport across this transect of Los Angeles, it is helpful to remember the underlying topography. As we move east across the network, elevations rise steadily from near sea level at RAN to over 250 m a.s.l. at CIT (Figure S3). This is relevant when considering that the Eaton fire broke out at an elevation of ∼600−700 m a.s.l.

https://doi.org/10.1021/acsestair.5c00430
ACS EST Air XXXX, XXX, XXX−XXX

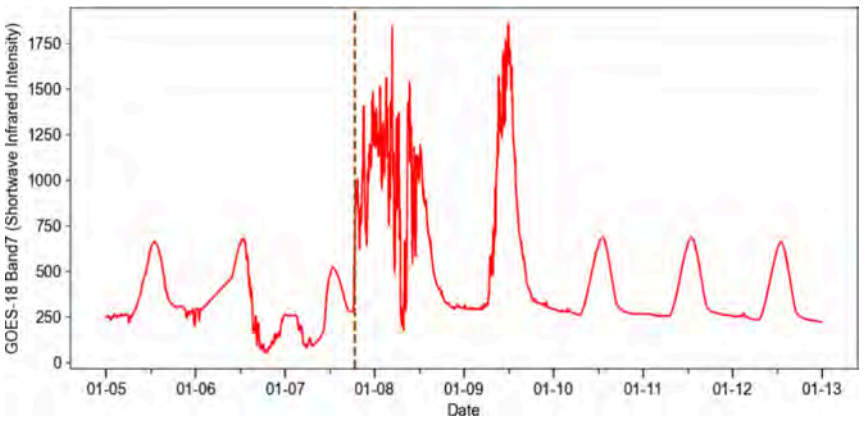

Figure 3. Intensity of SWIR emanating from the Eaton fire across the period of greatest fire destruction. The maroon dashed line indicates the time of the outbreak of the Eaton fire. Note that the SWIR image shown here is unitless. The spatial domain over which this figure was constructed is shown in Figure S4.

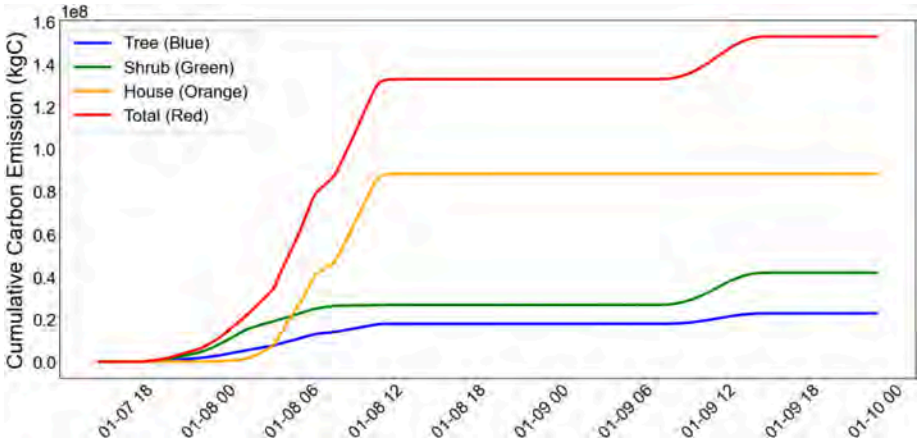

Figure 4. Hourly time series showing the carbon emissions resulting from the Eaton fire, separating the quantity released from burning tree canopies, shrubs, and structures.

before spreading both uphill to the San Gabriel mountains and downhill to the town of Altadena.

RESULTS AND DISCUSSION

Meteorological Context

Figure 2 shows how the meteorology at the onset of the fires (January 7th) was distinct in a number of interconnected ways: (1) the wind speed rose sharply on the 7th and remained elevated throughout the following day; (2) the wind direction stayed around 30° (indicating north−northeasterly winds); (3) the boundary layer expanded to a height of nearly 2 km, implying intense atmospheric mixing; (4) the average nighttime temperature remained ∼10 °C higher than in the previous and succeeding nights; and (5) concurrent with this elevated temperature, relative humidity dropped and stayed low. Summarizing the above, this sudden increase in northeasterly winds, carrying warm, dry air over the city, exacerbated the potential for wildfires to ignite and contributed to their spread as well as the dispersion of airborne constituents.

Variability in Fire Intensity and Combustion Material

In order to understand how the rate of combustion evolved as the wildfires progressed, we assess the SWIR intensity emanating from the Eaton fire at a 5 min resolution. From this output, we are able to quantify the relative magnitude of the fires' intensity throughout the burn period (Figure 3).

Prior to and following the days of intense burning, SWIR follows a diurnal pattern linked to regular surface temperature variations between daytime and nighttime. On the evening of January 7th, however, its magnitude rises sharply concurrent with the inception of the Eaton fire. This fire then burned intensely in the daytime hours of January 8th, briefly eased in the nighttime and early morning of the 9th, resurged strongly over the following day, and finally subsided on the 10th. While there was undoubtedly burning and smoldering that continued beyond the evening of January 9th, SWIR indicates that the most intense burning occurred in two pulses.

We also consider this evolution through the lens of the type of material that is being combusted. Following the methods outlined in the Supporting Information, we assess the land use of the region affected by the Eaton fire; assign tree, shrub, and structure carbon densities to the areas burned; and calculate total carbon emissions over time (Figure 4).

Demonstrating coherence with SWIR observations, Figure 4 shows how the destruction is partitioned into two distinct burn events. The first event (on January 8th) consumed approximately 2000 acres of vegetation in the lower hillside and 300 acres of homes in Altadena (considering only the acreage of the building roof area and not the surrounding infrastructure or property). A minor slowdown in carbon emissions on the morning of January 8th is then consistent with the brief drop in SWIR detected at the same time shown

https://doi.org/10.1021/acsestair.5c00430
ACS EST Air XXXX, XXX, XXX−XXX

Table 3. Average Concentrations and Standard Deviations of All Relevant Species (Plus the Ratio of CO:CO_2 Enhancements) across Both the CC and LAMC Networks in the Week Preceding the Wildfires

	CH_4 (ppb)		CO (ppb)		CO_2 (ppm)		CO_{xs}:$CO_{2,xs}$ (ppb/ppm)		$PM_{2.5}$ ($\mu g/m^3$)	
Network	Mean	STD	Mean	STD	Mean	STD	Mean	STD	Mean	STD
CC			503	160	516	50.0	2.95	0.28	11.6	8.28
LAMC	2440	270	443	226	491	36.9	5.05	1.02		

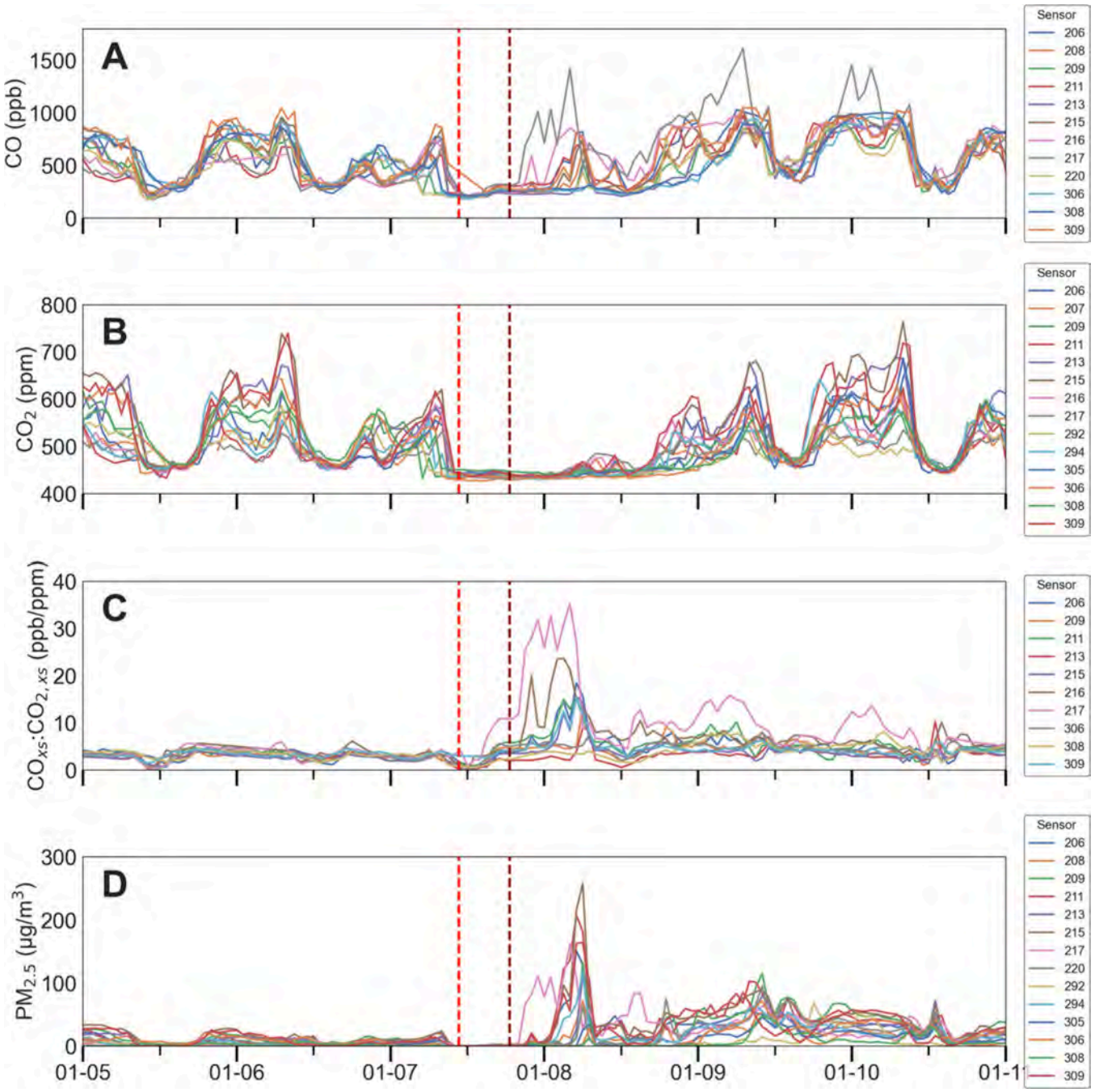

Figure 5. Concentrations of CO (A), CO_2 (B), CO_{xs}:$CO_{2,xs}$ (C), and $PM_{2.5}$ (D) in the days immediately preceding and following the outbreaks of the Palisades (red dashed line) and Eaton (maroon dashed line) fires at each relevant CC node listed in Table 1. Each color corresponds to a different CC node, which we subsequently explore individually in the following figures.

in Figure 3, indicating a temporary reduction in fire activity. The second event (on January 9th) consumed roughly 3000 acres of vegetation in the upper hillside, mainly shrubs and some trees. Notably, the carbon density of structures is much higher than that of tree canopies or shrubs; as such, the initial burn period resulted in a greater amount of total carbon emissions. We are then interested in assessing how much CO_2 and CO were generated by these fires and how this evolution

https://doi.org/10.1021/acsestair.5c00430
ACS EST Air XXXX, XXX, XXX−XXX

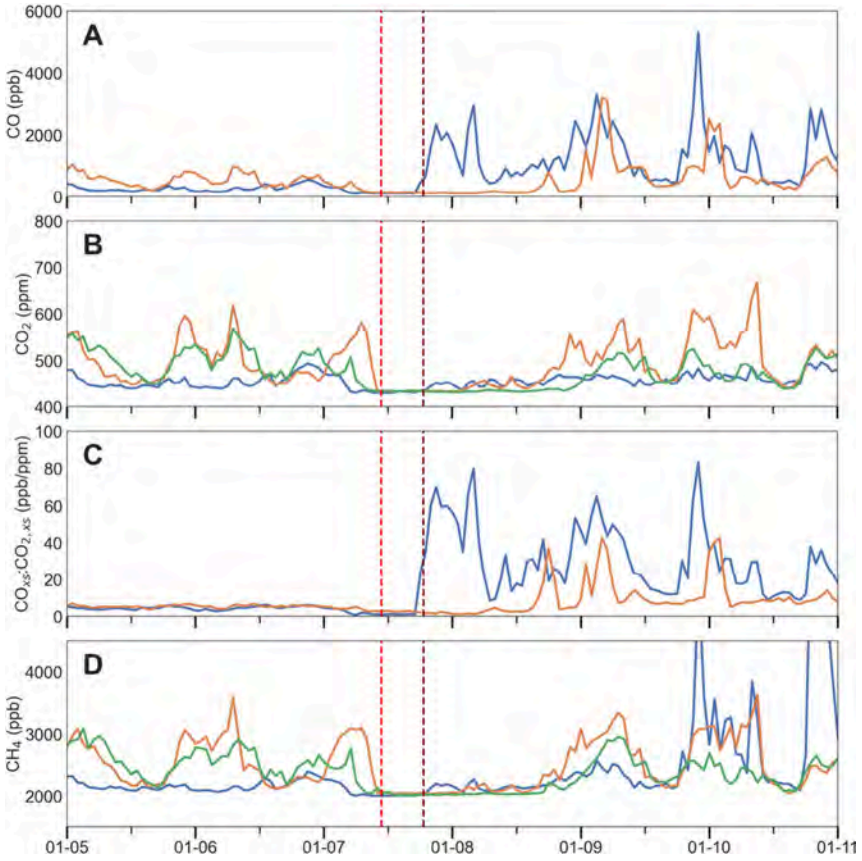

Figure 6. Concentrations of CO (A), CO_2 (B), CO_{xs}:$CO_{2,xs}$ (C), and CH_4 (D) in the days immediately preceding and following the outbreaks of the Palisades (red dashed line) and Eaton (maroon dashed line) fires at CIT (blue), USC (green), and RAN (orange).

in combustion material influenced atmospheric pollutant concentrations.

Bottom-Up Carbon Emissions Estimation

In the Supporting Information, we outline the precise methods we use to estimate the total amount of carbon released by the Eaton fire via a bottom-up approach. Briefly, this involves a quantification of the total acres of trees, shrubs, and structures burned combined with estimates of the carbon density of each of these materials. In later sections, we compare this calculation to estimates from a plume dispersion emission model.

Considering the entirety of the burned materials, we arrive at an estimate for the amount of carbon emitted from the Eaton fire of $(1.53 \pm 0.4) \times 10^8$ kg-C. We seek to put this number into context by comparing its magnitude to average anthropogenic contributions. A review of literature suggests that the mass of CO_2 released during wildfire events can be roughly 10× that of CO.[23−25] We note that there can be substantial differences in this emission ratio depending on the combustion efficiency of the wildfire and the extent to which emissions are a product of smoldering or flaming. We also note that the studies we cite were based on wildfires, and the combustion of nonvegetation material at the WUI is likely to feature different emission ratios of these pollutants.[26,27] Nevertheless, we proceed with this uniform value to obtain an order-of-magnitude estimate.

Applying this ratio of 10 to our estimate and converting from kg of C to kg of CO and CO_2, we arrive at values of $(4.9 \pm 1.3) \times 10^7$ kg of CO and $(4.9 \pm 1.3) \times 10^8$ kg of CO_2 for the total emitted from the Eaton fire. Given that these pollutants were predominantly released over a period of 2 days, we derive time-averaged emission rates of $(2.5 \pm 0.7) \times 10^7$ kg-CO/day and $(2.5 \pm 0.7) \times 10^8$ kg-CO_2/day.

For quantification of anthropogenic CO emissions, we turn to the California Emission Projection Analysis Model (CEPAM), managed by the California Air Resources Board (CARB) (https://ww2.arb.ca.gov/cepam). This source estimates anthropogenic CO emissions for the year 2024 across the entirety of LA County at 8.5×10^5 kg-CO/day. Therefore, we can infer that the CO emission rate from the Eaton fire was 21.2−37.6 times greater than the daily average anthropogenic contribution across the county.

Considering CO_2, we use the Hestia emission inventory developed by Gurney et al.[28] This inventory estimates fossil fuel-related emissions of CO_2 across LA county in 2011 to total 26.42 Mt-C/year, or 2.7×10^8 kg-CO_2/day. As such, the rate of CO_2 emissions from the Eaton fire is roughly 0.9−1.2 times that of the typical anthropogenic contributions. This comparison highlights how the Eaton fire was a relatively much more important source of CO than CO_2 (but nevertheless highly impactful to the abundance of both species). Finally, it is important to note that these comparisons between the wildfire emissions (estimated from our bottom-up investigation) and anthropogenic emissions (estimated from inventories) are distinct from the subsequent analyses we undertake to consider changes in the concentration enhancements of CO and CO_2, which are instead based on observational data.

https://doi.org/10.1021/acsestair.5c00430
ACS EST Air XXXX, XXX, XXX−XXX

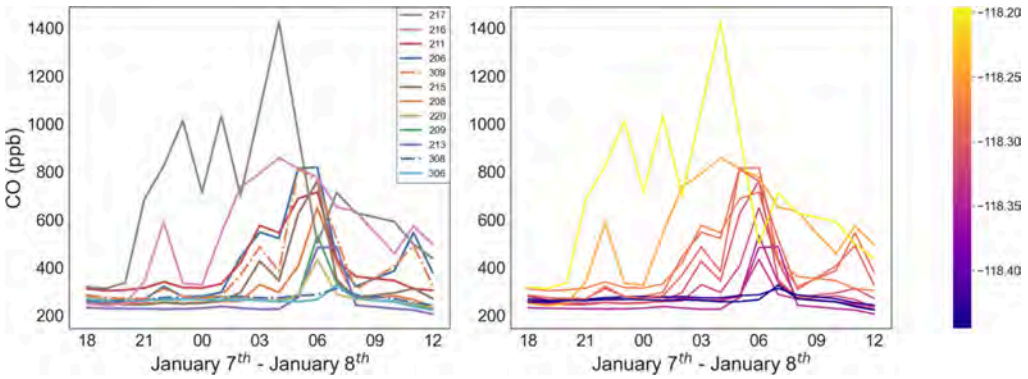

Figure 7. Initial detection of wildfire CO across the CC network. Left panel shows nodes labeled by their ID number (listed from East to West); right panel shows nodes color-coded by their longitude. Note, the Eaton fire began between 18:00 and 19:00 on January 7th.

Baseline Air Quality Conditions and Onset Period

Baseline statistics across both networks in the week preceding the outbreak of the fires (January 1st–January 7th) are presented in Table 3. We provide these values as points of comparison for the deviations in concentrations that we observe during the fires. For the calculation of the relative enhancement of CO to CO_2 over the background (denoted as CO_{xs}:$CO_{2,xs}$), we find this ratio by first subtracting from each species' observed concentration the minimum value registered on January 7th. The unique meteorology present on January 7th allows us to discern the true regional background levels for these three pollutants, which we round to 190 ppb for CO, 420 ppm for CO_2, and 2000 ppb for CH_4.

Northeasterly winds began blowing strongly in the morning on January 7th (Figure 2A) and were accompanied by a rapid expansion of the BLH (Figure 2C). As a result, ambient concentrations of CO, CO_2, CH_4, and $PM_{2.5}$ dropped sharply, as seen by both the CC (Figure 5) and LAMC (Figure 6) networks. This initial "reset" to background conditions provides a convenient way to gauge the subsequent spread of emissions from the fires. At the time the Palisades fire broke out (marked by a red dashed line in Figures 5 and 6), neither network detected increases in concentration of the monitored pollutants. This is consistent with what we were able to observe from the satellite imagery, namely, that emissions from the Palisades fire were not initially carried into the city (Figure S1). On the other hand, the onset of the Eaton fire (marked by a maroon dashed line on Figures 5 and 6) had an almost immediate impact. As evidenced by the spike in concentrations of CO and $PM_{2.5}$ across the CC network, emissions from the Eaton fire were felt across the city over the evening and early morning between January 7th and 8th. Readings from the LAMC network are also consistent with our understanding of smoke transport, as the CIT site (closest to the Eaton fire) saw a substantial increase in CO at this time, whereas the RAN site (furthest from the Eaton fire) did not.

The ratio of excess CO to CO_2 (CO_{xs}:$CO_{2,xs}$) was highest on the first day of burning (Figures 5C and 6C) indicating the large input of CO relative to that of CO_2. CO_2 concentrations remained low across both networks in concurrence with the period of high CO values. This is consistent with our bottom-up estimates for the production of CO and CO_2 from the Eaton fire relative to anthropogenic contributions; the increase in the level of CO over background levels was significantly higher.

Spatiotemporal Evolution of CO

The first spike in CO concentrations was detected at the easternmost node in the CC network (217) between 8 and 9 p.m. local time on January 7th, approximately 2 h after the inception of the Eaton fire (Figure 7, left). Subsequently, CC sensors track how this initial plume was transported westward, with each successive peak decreasing in magnitude as time passes. Color-coding our time series by site longitude highlights this spread as the night of January 7th progressed to the early morning of January 8th (Figure 7, right).

The dilution associated with this transport is due to both horizontal and vertical dispersion of the smoke plume, given that the Eaton fire broke out at a higher elevation than that of the CC nodes (Figure S3). Also, the axis of wind transport is askew with respect to the orientation of the CC array (Figure 1). CC node 217 is situated approximately 20 km southwest of the Eaton fire outbreak. At this time, wind over the region was blowing at roughly 5 m/s (18 kph) and coming from ~30°. This helps explain why excess CO is registered at site 217 much earlier than at the other CC sites (Figure 1). The encroachment of smoke over the city is slower than the movement of smoke along the principal wind axis. It took another 4–6 h before elevated CO was registered at sites in downtown LA. Finally, CC sites at the western end of the network (306 and 308) only see a very minor enhancement in CO around 7 a.m. on the morning of January 8th. It is important to note that this dilution is occurring concurrent with (and despite) the nighttime boundary layer continuing to contract (Figure 2C). Upon its subsequent re-expansion, beginning on the morning of January 8th, concentrations drop in unison across the whole network. We note that corroborating our ERA5 reanalysis BLH values with real-world measurements would strengthen this analysis but were unable to procure direct observational evidence for the spatiotemporal domain in question. Nevertheless, the agreement in the response of pollutant concentrations to modeled BLH values gives us confidence in their general accuracy.

The rapid dilution of CO emanating from the Eaton fire is also discernible when we consider concentrations at the CIT and RAN. The CIT site is located just over 8 km from the Eaton fire outbreak, and we detect elevated CO here very shortly after the reported outbreak. The magnitude of the peak is also roughly double that seen by any other node in the CC network. On the other hand, the RAN site, more than 40 km away from the Eaton fire outbreak, senses only the slightest deviation from baseline on this night, an increase of merely 50

https://doi.org/10.1021/acsestair.5c00430
ACS EST Air XXXX, XXX, XXX–XXX

ppb, at approximately 8 a.m. on January 8th (again, consistent with our interpretation that it did not experience emissions from the Palisades fire on this first night).

The difference in maximum and minimum CO concentrations (ΔCO) seen by sensors in both networks on this first 24 h of the Eaton fire varies as a function of distance from the fire outbreak (Figure 8). By fitting an exponential curve to these observations, we can then estimate that concentrations at the origin of the outbreak might have reached peak values above 6000 ppb. This empirically fitted exponential function helps highlight the rapid dilution of smoke as the plume travels downwind and downhill. This one-dimensional representation of dilution is incomplete, given what we know about the axis of smoke transport relative to our sensor array. We utilize this visualization as an initial attempt to document the spread of pollutants, and in subsequent sections, we expand on this by considering a more sophisticated two-dimensional dispersion analysis.

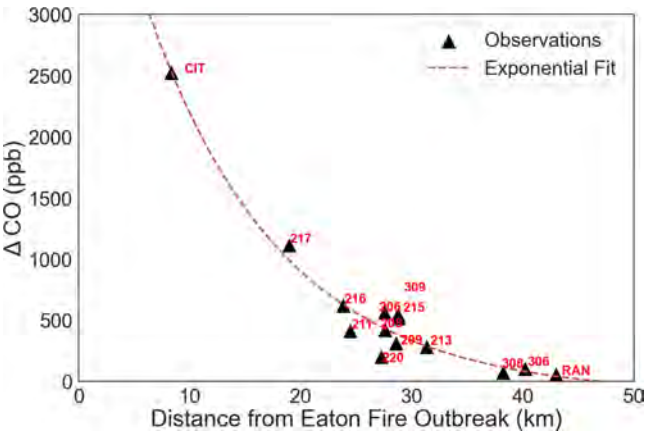

Figure 8. Maximum enhancement in CO (relative to the minimum value observed on January 7th) experienced across the CC and LAMC networks in the first 24 h following the outbreak of the Eaton fire as a function of absolute distance from the origin.

Following this first day of steady northeasterly winds, increases in the level of CO across the CC network cease to follow a consistent spatial pattern. By January 11th, CO concentrations return to prefire conditions. This is consistent both with the timeline established in our satellite imagery investigation of burning as well as with the fire expansion progression reported by Cal Fire.[29]

Spatiotemporal Evolution of $PM_{2.5}$

The general patterns that we witness in the evolution of CO are also reflected in $PM_{2.5}$ concentrations (Figure 9). An increase over the baseline is first detected at the easternmost node reporting $PM_{2.5}$ (217), also between 8 and 9 p.m. local time on January 7th. Subsequently, increases in $PM_{2.5}$ are detected in downtown LA between 2 and 3 a.m. (January 8th) before reaching the sensors closest to the coast around 7 a.m. As with CO, as the smoke plume spreads westward, successive peak concentrations mostly decrease in magnitude. One notable difference between the trends we see in CO versus $PM_{2.5}$ is that site 217, the first to detect an enhancement, does not reach the highest overall concentrations. The reason for this is not immediately clear, but we do not exclude the possibility that the sensor at site 217 was simply performing at a lower sensitivity, as is sometimes the case with low-cost instruments. Nevertheless, the spatial pattern is clearly indicative of the meteorological circumstances conducive to the rapid dispersion of pollutant emissions.

For the rest of the fire period, $PM_{2.5}$ concentrations did not exceed the peaks achieved on this first night (Figure 10). Still, $PM_{2.5}$ remained elevated over typical conditions until January 11th, again consistent with the period of the most intense burning.

Trends in the Ratio of $PM_{2.5}$:CO Concentrations

Concentrations of $PM_{2.5}$ in the first three days following the fire do not respond to typical diurnal trends (Figure 5). Unlike CO concentrations, which drop in the daytime and swell in the nighttime as the boundary layer expands and contracts, $PM_{2.5}$ levels do not show consistent diurnal patterns. One possible explanation for this is that we are witnessing enhanced production of secondary aerosols during daylight hours. Biomass burning is known to produce large amounts of volatile organic compounds (VOCs), and previous studies have outlined how the transformation of these compounds to secondary aerosols can constitute a significant fraction of the total organic carbon released in wildfires.[30−35] If the rate of production increases in the daytime on account of higher temperatures and greater abundance of photochemically-derived oxidizing agents such as ozone or hydroxyl radicals, it would explain why we might not see the same midday drop in $PM_{2.5}$ as we do for CO.

We consider how the ratio of $PM_{2.5}$ to CO evolves in the days following the outbreak (Figure 11). The sharp peaks occurring right around noon of the 9th, 10th, and 11th of

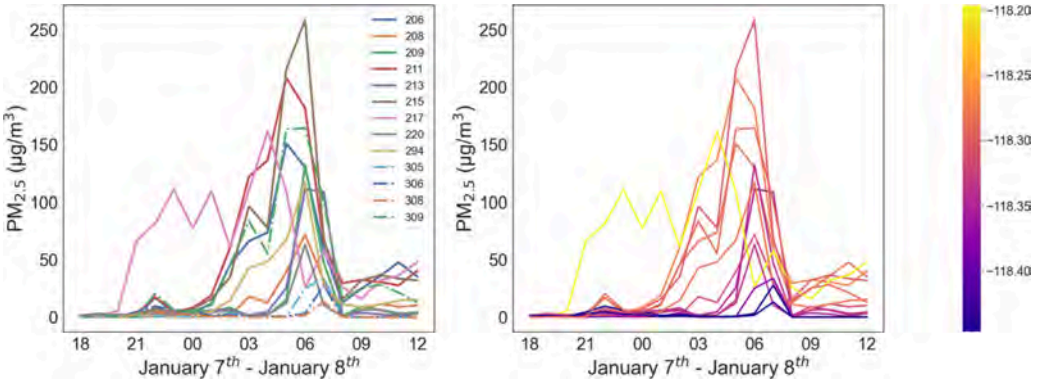

Figure 9. Initial detection of wildfire $PM_{2.5}$ across the CC network. Left panel shows sites labeled by their ID number; right panel shows sites color-coded by their longitude. Note, the Eaton fire began between 18:00 and 19:00 on January 7th.

https://doi.org/10.1021/acsestair.5c00430
ACS EST Air XXXX, XXX, XXX−XXX

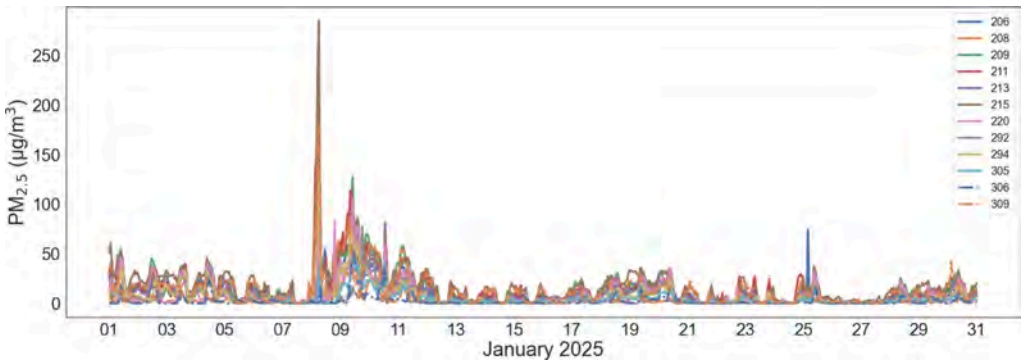

Figure 10. $PM_{2.5}$ concentrations across the CC network for the month of January 2025.

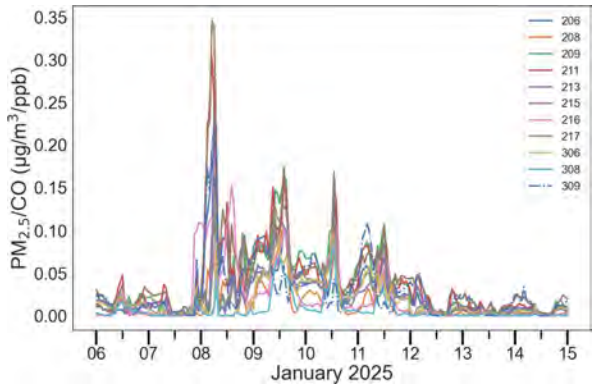

Figure 11. Ratio of $PM_{2.5}$:CO concentrations across the CC network in the days surrounding the Eaton fire outbreak.

January point to the persistent enhancement in $PM_{2.5}$ that resists the midday dilution that CO is experiencing. The gradual decrease in the daily maxima reached could suggest a slowing of $PM_{2.5}$ production as the aerosol precursor emissions from the fire subside.

We also directly examine the correlation between $PM_{2.5}$ and CO concentrations as a function of time of day (Figure 12). Analyzing the period of January 7, 2025 18:00 to January 14, 2025 18:00 (i.e., one week following the Eaton fire inception), we separate our observations into midday hours (9−3 p.m.) and midnight hours (12−6 a.m.). Taking the slope across these two periods demonstrates how the daytime enhancement of $PM_{2.5}$ relative to that of CO is much higher and more statistically significant. This is consistent with $PM_{2.5}$ production being highest in the daytime, but we are unable to definitively conclude that this hypothesis adequately explains our observations, as additional meteorological factors and variations in primary $PM_{2.5}$ emissions could also be at play here. We nevertheless present this analysis to motivate future investigations interested in continuing to assess the impact of wildfire emissions on secondary $PM_{2.5}$ formation.

Indirect Fire Impacts—Atypical Emissions

Aside from the direct emissions resulting from the combustion of vegetation and structures, the destruction of utility gas infrastructure caused by the wildfires also led to significant amounts of methane being released into the atmosphere. Out of the 38,608 households impacted by the Eaton Fire, nearly 80% utilized natural gas for heating (https://incidents.fire.ca.gov/media/1lqbnqmi/eaton-fire-demographics.pdf). Disruptions to this infrastructure were detected shortly after the fire spread to the residential area of Altadena, and the SoCalGas utility company first announced service shut offs on the

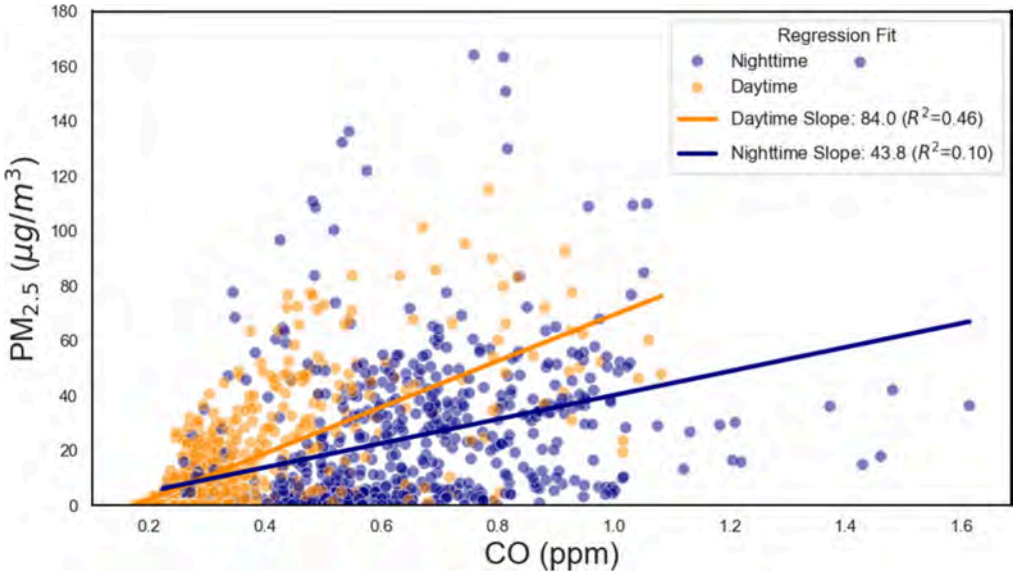

Figure 12. Correlation between $PM_{2.5}$ and CO concentrations across the CC network in the week following the Eaton fire outbreak, separated by daytime and nighttime.

https://doi.org/10.1021/acsestair.5c00430
ACS EST Air XXXX, XXX, XXX−XXX

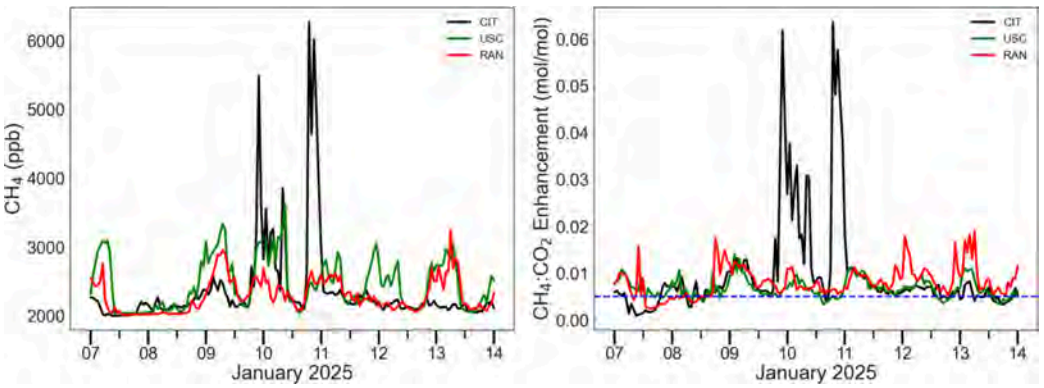

Figure 13. Methane concentrations (left) and CH_4:CO_2 enhancement ratios (right) across the LAMC network immediately following the fire outbreak. The blue dashed line depicts a baseline ratio derived from past literature.

afternoon of January 10th.[36] We are able to independently verify these fugitive CH_4 emissions from measurements taken at CIT, which show a spike starting on the evening of January 9th and a resurgence on January 11th (Figure 13, left). After this, no significant peaks were detected for the rest of the wildfire period at this site. Unlike the dissipation of concentrations we saw in examining CO, this methane plume detected at CIT does not register with similar intensity at USC or RAN. This further indicates the source as localized to the Pasadena area and reflects the shifting meteorological conditions, given that by January 9th, the strong westerly Santa Ana winds had subsided (Figure 2).

To take into account the influence of the BLH and to normalize for meteorological impacts on methane concentrations, we consider the enhancement ratios of CH_4 to CO_2. To derive these ratios, we again use the concentrations achieved on the evening of January 7th as indicative of the regional background and compute the difference between this baseline over time. We also compare these enhancements to what one might expect from the reported wildfire emission ratios (Figure 13, right).

Even after correcting for meteorology, the signal seen at CIT between January 10th−11th remains highly pronounced. In past work examining wildfire plumes from satellite measurements, the ratio of CH_4:CO_2 emissions is estimated to be ∼0.005 mol/mol.[37] Similarly, a study utilizing in situ measurements estimates the CH_4:CO_2 emission ratio from the burning of temperate forests to be ∼0.007 mol/mol,[38] confirming sufficient agreement with satellite estimates. At CIT, however, the enhancement ratio reaches 10× that amount, indicating that the methane emissions do not originate from combustion processes. We note that measurements of ethane concentrations would allow us to further corroborate this claim by assessing the ratio of ethane to methane (which varies comparing biomass burning and natural gas leaks), but we were unable to procure such measurements. Still, the temporal delay between the outbreak of the Eaton fire and the first detection of elevated CH_4 is also indicative that it was not the fire itself producing the methane but rather its impacts on natural gas infrastructure. Previous studies have posited on the theoretical potential for wildfires to threaten natural gas infrastructure,[39,40] but we are unable to find reports of direct observational evidence in the literature. This event thus represents an important case study for assessing the prevalence and impact of gas leaks during urban wildfires. As late as January 31st, mobile monitoring conducted by the South Coast Air Quality Management District was still able to capture hot spots of methane in Altadena,[41] suggesting that the these leaks extended past the end of the wildfires themselves. Given that CH_4 has a much higher global warming potential than that of CO_2, quantifying the total amount of fugitive methane released as a result of urban wildfires will be an important consideration for subsequent studies looking to fully capture the climatic impacts of wildfires.

Modeling CO Emissions from the Eaton fire

We have outlined how the Eaton fire consisted of two distinct pulses of burning (Figure 3), the first event was unique in that it occurred during a period of intense atmospheric mixing, consumed structures as well as vegetation, and affected areas at a lower elevation than the second event. Normalizing for atmospheric dilution, we take the product of concentration and boundary layer height to arrive at a column density of CO at the CIT site, nearest the fire (Figure 14), thus illustrating how CO production was maximal during the early stages of burning.

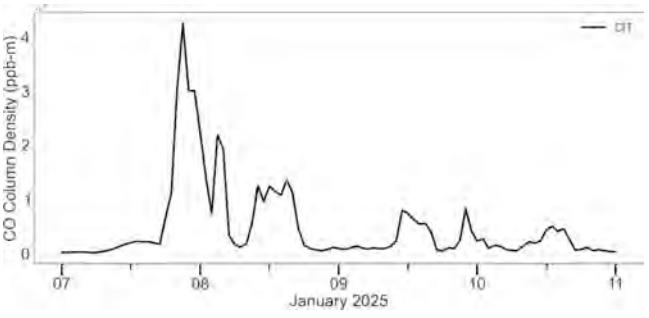

Figure 14. Column density of CO at CIT as calculated by the product of concentration and BLH. Note that the *y*-axis is scaled by a factor of 10^6.

Here we consider a model of how this plume of excess CO spread across downtown and west-side Los Angeles. The exponential decrease in maximal CO enhancement with distance during this first burn period (Figure 8) suggests that the initial plume emitted from the Eaton fire spread in a Gaussian manner.[42] We use a simple model (eqs 1 and 2) to test this premise, now in two dimensions:

$$C(x, y) = \frac{E}{4\pi Dr} \exp\left[\frac{-u(r - (x - x_0))}{2D}\right] \quad (1)$$

https://doi.org/10.1021/acsestair.5c00430
ACS EST Air XXXX, XXX, XXX−XXX

$$r = \sqrt{(x - x_0)^2 + (y - y_0)^2} \quad (2)$$

where C is the observed CO enhancement (ppb) at sites located x kilometers from the fire origin and off the center-line of the plume by y kilometers (Figure 15). E is the CO emission

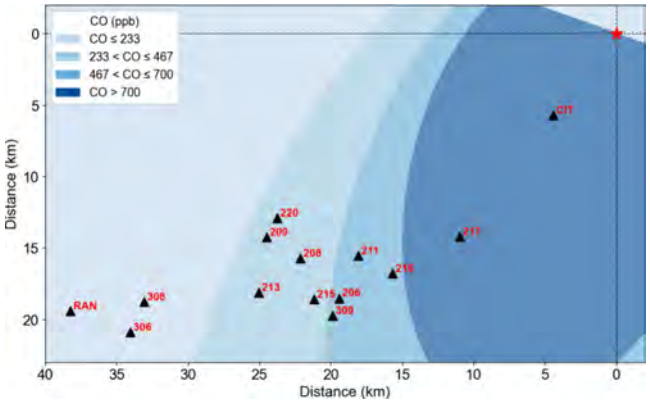

Figure 15. Sensor locations plotted with respect to their 2D distances from the Eaton fire origin (shown as the red star), as described above. The background color then represents the modeled CO concentrations.

rate, originally expressed in ppb·m^3/s but converted into kg-CO/h using the ideal gas law under standard conditions. D is the effective diffusivity (m^2/s), and u is the mean wind speed in the direction of transport (m/s). The fire location (x_0, y_0) is then set as (0, 0).

We minimize the RMSE by fitting model values of the predicted CO enhancements to observations taken at our measurement points across both networks. Here, we do not attempt to model the evolution of the plume in time but rather seek to only consider the greatest enhancements achieved during the first pulse of burning as a function of distance. Inherent in this model is the assumption of constant wind speed (5.5 m/s, Figure 2A), constant plume travel direction (along prevailing winds, Figure 2B), and constant diffusivity. The best fit model output (with an RMSE of 70 ppb) is shown in Figure 16, and calls for a diffusion coefficient (D) of 0.02 km^2/s and an emission rate (E) of 2×10^7 kg-CO/h.

The validity of this estimate for D can be evaluated by using our observations. The RAN station lies ∼30 km off the main downwind axis, for which the inferred diffusivity implies a transport time of ∼12.6 h. This closely matches the observed

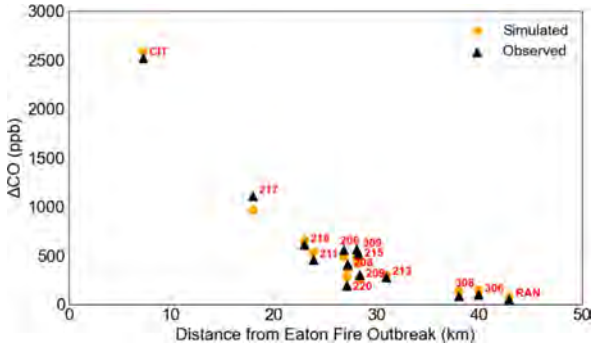

Figure 16. Analogous to Figure 8 but including model results from the solution of eq 1.

∼13 h delay between fire ignition and the first (albeit minor) enhancement in CO seen at RAN (Figure S11).

During the first 18 h of burning, when emissions rose most rapidly (Figure 4), our bottom-up estimate yields an approximate rate of $(2.3 \pm 0.6) \times 10^6$ kg-CO/h. As such, we find modest agreement (within 1 order of magnitude) with our model results.

In the SI, we provide details of a more sophisticated plume model that takes into account dispersion in three dimensions. Including the z-axis is relevant because the burning occurred at a higher elevation than our points of measurement. We explore three cases of this 3-D model: (1) fixing the emission height, wind speed, and wind direction to constant values, (2) allowing the emission height to vary, and (3) allowing both the emission height and the wind direction to vary. Beginning with a fixed emission height of 500 m (as a rough estimate of the Eaton fire elevation, Figure S3), we find that in the subsequent model simulations, the optimal height deviates only slightly, settling at 496 m in case 2 and 457 m in case 3. This result is consistent with our understanding of where the fire spread on the first day of burning and again points to the burning of the residential areas of Altadena as the greatest sources of CO (relative to the burning of shrubland at much higher elevations on the subsequent day). Similarly, allowing the wind direction to vary results in variability of only ∼8°, supporting the general accuracy of the modeled wind field and the consistency of the direction from which the wind was blowing at this time. Across these three model evaluations, we achieve RMSEs of 61−64 ppb and predict emission rates of $(6.7-8.1) \times 10^5$ kg-CO/h. This 3-D model, with more adjustable parameters, performs slightly better in terms of fitting the observed data relative to the 2-D model and estimates an emission rate of CO within a factor of 2−4 of our bottom-up estimate. We acknowledge that both approaches (bottom-up calculation and dispersion modeling) are highly simplified and not fully representative of real-world conditions. Nevertheless, we find the relative agreement achieved here adds confidence to both methodologies. Corroborating the results of our bottom-up estimate is first relevant for verifying the total amount of carbon released from this fire. Improving our understanding of how wildfires impact the global carbon budget will continue to be an important goal going forward. Second, using CO as a proxy to visualize the spread of a smoke plume is relevant for understanding the transport of all wildfire pollutant emissions, including those species which we do not have the capabilities to measure. These results therefore contribute to elucidating how exposure risks vary as a function of the distance from a fire outbreak.

Public Exposure Implications

The spatiotemporal trends in CO and $PM_{2.5}$ concentrations that we describe in previous sections highlight the significant hyperlocal variability in how urban wildfires affect their surrounding domains. The EPA National Ambient Air Quality Standards (https://www.epa.gov/criteria-air-pollutants/naaqs-table) set a 24 h threshold of 35 μg/m^3 for $PM_{2.5}$ concentrations and an 8 h threshold of 9 ppm for CO as criteria for identifying when air quality becomes harmful to human health. Because our sensors do not register exceedances of the CO threshold, we focus here solely on $PM_{2.5}$. We note that one site (215) experienced 3 days in exceedance, four sites (206, 211, 217, and 309) experienced 2 days in exceedance, four sites (209, 213, 220, and 294) experienced 1 day in

https://doi.org/10.1021/acsestair.5c00430
ACS EST Air XXXX, XXX, XXX−XXX

exceedance, and the remainder experienced none (Figure 17). To put these values into context, we compare these

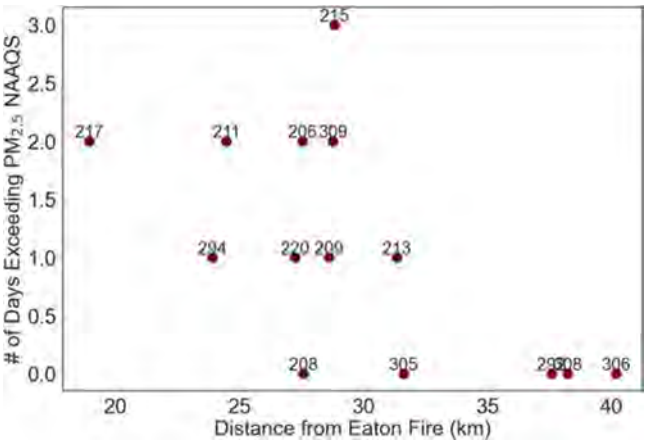

Figure 17. Number of days when $PM_{2.5}$ exceeded 35 $\mu g/m^3$ for a 24 h period as recorded by the CC sensors.

exceedances to those listed in the yearly SCAQMD reports (https://www.aqmd.gov/home/air-quality/historical-air-quality-data/historical-data-by-year). In the preceding year, 2024, central LA is reported to have experienced 5 days in total exceeding the 35 $\mu g/m^3$ threshold. Across both of 2022 and 2023, however, no exceedances were registered. As such, we can confirm that this fire had a notable impact on air quality relative to the past years.

There is only a modest relationship in the rate of exceedances versus the distance of each site to the Eaton fire. As the winds shifted in the days following the inception of the Eaton fire, PM concentrations became more well-mixed across the air basin. What is clear, however, is that the public health impacts of the fires may have been far greater had this injection of $PM_{2.5}$ been emitted and produced under less intense meteorological conditions (which helped push the Palisades fire emissions directly offshore). The peak in $PM_{2.5}$ concentrations occurred concurrently, and in spite of, a BLH roughly twice its typical magnitude (Figure 2C). It is therefore interesting to contemplate that the high winds occurring at this time were primary drivers of the fire's inception but also contributed to lessening the atmospheric impact of the resulting pollutant emissions.

SUMMARY

In this study, we examine the impact of the January 2025 Los Angeles wildfires from a variety of perspectives. We first consider how satellite imaging can aid in tracking the development of wildfires, the temporal changes in their intensity, and the type of land being affected. Doing so, we corroborate bottom-up estimates of pollutant emissions with real-time air quality measurements and meteorological plume dispersion models. We thus highlight how the integration of high-spatial-resolution, low-cost sensor networks with lower-spatial-resolution, high-grade instruments can provide a more nuanced understanding of pollutant transport and dilution during extreme emission events.

Carbon emissions from the Eaton fire were dominated by the destruction of homes rather than the burning of trees and shrubs. Our bottom-up estimates imply that the Eaton fire generated CO at rates that exceed daily anthropogenic CO emissions in the greater Los Angeles area by a factor of 21.2–37.6. Additionally, the dispersion of CO followed a Gaussian distribution such that the spread of pollution was predictable and indicated transport into the city over the course of 4–12 h. Our plume modeling, evaluated in both two and three dimensions through comparisons with observational evidence, resulted in predicted emission rates which agreed with our bottom-up estimate within an order of magnitude, further helping constrain our quantification of the total carbon lost to combustion.

Across the year, winds in Los Angeles are predominantly westerly, blowing inland from the ocean. However, Santa Ana winds are common in the late fall and winter, bringing warm, dry air from the interior (N–NE) to the city. As we have seen in this case study, shifting wind patterns play a crucial role in modulating the spread of pollutants. Because the fire season in Southern California is projected to continue expanding with rising temperatures in the region,[43] modeling the dispersion of wildfire emissions across a variety of different meteorological scenarios will be an important tool for informing public health strategies to minimize exposure. Additionally, warmer temperatures are associated with increased atmospheric stagnation, which would further exacerbate the impact of pollutant emissions.[44] In the context of these evolving environmental conditions, we underscore the continued importance of multipoint air quality monitoring, not only for providing real-time information to communities but also for improving our modeling capabilities.

As the Carbon Census network continues to expand, its orientation along this critical transect of Los Angeles (Figure 1), parallel to typical daytime winds, will enhance our ability to describe how air masses evolve as they travel over large population centers with myriad sources of emissions. The integration of higher quality data collected with more sophisticated instruments, such as those used by the LAMC network, validates our low-cost instruments and establishes conditions beyond our domain's boundary. This, combined with satellite observations, allows us to provide a cohesive picture of atmospheric events pertinent to public exposure. Through this study, we demonstrate the functionality of our holistic approach and help guide future analyses of wildfire events that are estimated to grow in frequency and severity.

ASSOCIATED CONTENT

Supporting Information

The Supporting Information is available free of charge at https://pubs.acs.org/doi/10.1021/acsestair.5c00430.

Eaton LA area wildfire plume satellite image; modeled and measured wind speed agreement plot; sensors' relative positions and elevations plot; estimation methodology for burned area and total amount of carbon lost; maps of fire region of interest and of difference in NDVI pre- and postfire; figures detailing training of land classification model; image showing structure area loss quantification methods; burned areas map from NVDI difference calculation; tables outlining bottom-up carbon emission rate estimate assumptions; 3-D Gaussian dispersion plume model methodology; figures contrasting the modeled diffusion rates and showing first CO enhancement following Eaton fire inception (PDF)

https://doi.org/10.1021/acsestair.5c00430
ACS EST Air XXXX, XXX, XXX–XXX

AUTHOR INFORMATION

Corresponding Author

Pietro F. Vannucci − *Department of Earth Sciences, University of Southern California, Los Angeles, California 90089, United States;* orcid.org/0000-0002-6137-3447; Phone: +1 (314) 489-3925; Email: pietrofv@gmail.com

Authors

Wenye Wang − *Department of Earth Sciences, University of Southern California, Los Angeles, California 90089, United States*

Jooil Kim − *Scripps Institution of Oceanography, University of California, San Diego, La Jolla, California 92093, United States*

Timothy Lueker − *Scripps Institution of Oceanography, University of California, San Diego, La Jolla, California 92093, United States*

William M. Berelson − *Department of Earth Sciences, University of Southern California, Los Angeles, California 90089, United States*

Complete contact information is available at: https://pubs.acs.org/10.1021/acsestair.5c00430

Notes

Safety Statement. No unexpected or unusually high safety hazards were encountered when conducting this study.
The authors declare no competing financial interest.

ACKNOWLEDGMENTS

We acknowledge USC for providing financial and other support in the form of a Presidents Sustainability Award and a Dornsife Public Exchange Grant. The Carbon Census array benefits from the ongoing collaborations provided by the UC Berkeley BEACO2N group led by Ron Cohen. Carbon Census installation, calibration, and upkeep were provided by Nick Rollins and Devan Roper at USC. Anna Karion at NIST and the broader Megacities group made sensor data available. Thanks to Alex Turner (U. Washington) for conversations about plume modeling. Qi Yi also provided helpful guidance regarding GIS.

REFERENCES

(1) Cunningham, C. X.; Williamson, G. J.; Bowman, D. M. J. S. Increasing Frequency and Intensity of the Most Extreme Wildfires on Earth. *Nat. Ecol. Evol.* **2024**, *8* (8), 1420−1425.

(2) Jain, P.; Castellanos-Acuna, D.; Coogan, S. C. P.; Abatzoglou, J. T.; Flannigan, M. D. Observed Increases in Extreme Fire Weather Driven by Atmospheric Humidity and Temperature. *Nat. Clim. Change* **2022**, *12* (1), 63−70.

(3) Jones, M. W.; Abatzoglou, J. T.; Veraverbeke, S.; Andela, N.; Lasslop, G.; Forkel, M.; Smith, A. J. P.; Burton, C.; Betts, R. A.; Van Der Werf, G. R.; Sitch, S.; Canadell, J. G.; Santín, C.; Kolden, C.; Doerr, S. H.; Le Quéré, C. Global and Regional Trends and Drivers of Fire Under Climate Change. *Rev. Geophys.* **2022**, *60* (3), No. e2020RG000726.

(4) Harries, M. E.; Allen, D. T.; Adetona, O.; Bell, M. L.; Black, M. S.; Burgess, J. L.; Dryer, F. L.; Holder, A. L.; Mascareñas, A.; Rosario-Ortiz, F. L.; Stec, A. A.; Turpin, B. J.; Zelikoff, J. T. A Research Agenda for the Chemistry of Fires at the Wildland-Urban Interface: A National Academies Consensus Report. *Environ. Sci. Technol.* **2022**, *56* (22), 15189−15191.

(5) Committee on the Chemistry of Urban Wildfires; Board on Chemical Sciences and Technology; Division on Earth and Life Studies; National Academies of Sciences, Engineering, and Medicine. *The Chemistry of Fires at the Wildland−-Urban Interface*; National Academies Press: Washington, D.C., 2022; p 26460. DOI: 10.17226/26460.

(6) Burke, M.; Driscoll, A.; Heft-Neal, S.; Xue, J.; Burney, J.; Wara, M. The Changing Risk and Burden of Wildfire in the United States. *Proc. Natl. Acad. Sci. U. S. A.* **2021**, *118* (2), No. e2011048118.

(7) Thilakaratne, R.; Hoshiko, S.; Rosenberg, A.; Hayashi, T.; Buckman, J. R.; Rappold, A. G. Wildfires and the Changing Landscape of Air Pollution-Related Health Burden in California. *Am. J. Respir. Crit. Care Med.* **2023**, *207* (7), 887−898.

(8) Burke, M.; Childs, M. L.; De La Cuesta, B.; Qiu, M.; Li, J.; Gould, C. F.; Heft-Neal, S.; Wara, M. The Contribution of Wildfire to PM2.5 Trends in the USA. *Nature* **2023**, *622*, 761.

(9) Cal Fire. *2025 Incident Archive*; The Department of Forestry and Fire Protection. https://www.fire.ca.gov/incidents/2025 (accessed 03 25, 2025).

(10) Barnes, C.; et al. *Climate Change Increased the Likelihood of Wildfire Disaster in Highly Exposed Los Angeles Area*; World Weather Attribution, 2025. https://www.worldweatherattribution.org/wp-content/uploads/WWA-scientific-report-LA-wildfires-1.pdf (accessed 03 31, 2025).

(11) Turner, A. J.; Kim, J.; Fitzmaurice, H.; Newman, C.; Worthington, K.; Chan, K.; Wooldridge, P. J.; Köehler, P.; Frankenberg, C.; Cohen, R. C. Observed Impacts of COVID-19 on Urban CO2 Emissions. *Geophys. Res. Lett.* **2020**, *47* (22), No. e2020GL090037.

(12) Delaria, E. R.; Kim, J.; Fitzmaurice, H. L.; Newman, C.; Wooldridge, P. J.; Worthington, K.; Cohen, R. C. The Berkeley Environmental Air-Quality and CO2 Network: Field Calibrations of Sensor Temperature Dependence and Assessment of Network Scale CO2 Accuracy. *Atmospheric Meas. Technol.* **2021**, *14* (8), 5487−5500.

(13) Fitzmaurice, H. L.; Turner, A. J.; Kim, J.; Chan, K.; Delaria, E. R.; Newman, C.; Wooldridge, P.; Cohen, R. C. Assessing Vehicle Fuel Efficiency Using a Dense Network of CO2 Observations. *Atmospheric Chem. Phys.* **2022**, *22* (6), 3891−3900.

(14) Patel, M. Y.; Vannucci, P. F.; Kim, J.; Berelson, W. M.; Cohen, R. C. Towards a Hygroscopic Growth Calibration for Low-Cost PM2.5 Sensors. *Atmospheric Meas. Technol.* **2024**, *17* (3), 1051−1060.

(15) Asimow, N. G.; Turner, A. J.; Cohen, R. C. Sustained Reductions of Bay Area CO2 Emissions 2018−2022. *Environ. Sci. Technol.* **2024**, *58* (15), 6586−6594.

(16) Winter, A. R.; Zhu, Y.; Asimow, N. G.; Patel, M. Y.; Cohen, R. C. A Scalable Calibration Method for Enhanced Accuracy in Dense Air Quality Monitoring Networks. *Environ. Sci. Technol.* **2025**, *59* (5), 2599−2610.

(17) Kim, J.; Berelson, W. M.; Rollins, N. E.; Asimow, N. G.; Newman, C.; Cohen, R. C.; Miller, J. B.; McDonald, B. C.; Peischl, J.; Lehman, S. J. Observing Anthropogenic and Biogenic CO2 Emissions in Los Angeles Using a Dense Sensor Network. *Environ. Sci. Technol.* **2025**, *59* (7), 3508−3517.

(18) Verhulst, K. R.; Karion, A.; Kim, J.; Salameh, P. K.; Keeling, R. F.; Newman, S.; Miller, J.; Sloop, C.; Pongetti, T.; Rao, P.; Wong, C.; Hopkins, F. M.; Yadav, V.; Weiss, R. F.; Duren, R. M.; Miller, C. E. Carbon Dioxide and Methane Measurements from the Los Angeles Megacity Carbon Project - Part 1: Calibration, Urban Enhancements, and Uncertainty Estimates. *Atmospheric Chem. Phys.* **2017**, *17* (13), 8313−8341.

(19) Kim, J.; Verhulst, K.; Lueker, T.; Salameh, P.; Cox, A.; Walker, S.; Paplawsky, B.; Prinzivalli, S.; Fain, C.; Stock, M.; DiGangi, E.; Biggs, B.; Angel, B.; Karion, A.; Pongetti, T.; Callahan, W.; Weiss, R. F.; Keeling, R. F.; Miller, C. E. In Situ Carbon Dioxide, Methane, and Carbon Monoxide Mole Fractions from the Los Angeles Megacity Carbon Project. *NIST Public Data Repository*; National Institute of Standards and Technology (NIST), 2021. https://data.nist.gov/od/id/mds2-2388 (accessed 03 25, 2025).

(20) National Oceanic and Atmospheric Administration (NOAA). *ABI Band 7 (3.9 μm)—Shortwave Infrared Band*. https://www.star.

https://doi.org/10.1021/acsestair.5c00430
ACS EST Air XXXX, XXX, XXX−XXX

nesdis.noaa.gov/GOES/documents/ABIQuickGuide_Band07.pdf (accessed 08 12, 2025).
(21) Hersbach, H.; Bell, B.; Berrisford, P.; Biavati, G.; Horányi, A.; Muñoz Sabater, J.; Nicolas, J.; Peubey, C.; Radu, R.; Rozum, I.; Schepers, D.; Simmons, A.; Soci, C.; Dee, D.; Thépaut, J.-N. ERA5 hourly Data on Single Levels from 1940 to Present. *Copernicus Climate Change Service (C3S), Climate Data Store (CDS)*, 2023. https://cds.climate.copernicus.eu/datasets/reanalysis-era5-single-levels?tab=overview (accessed 02 03, 2025).
(22) Historical Data Selector. *California Data Exchange Center, California Department of Water Resources*. https://cdec.water.ca.gov/dynamicapp/selectQuery (accessed 06 04, 2025).
(23) Ward, D. E.; Hardy, C. C. Smoke Emissions from Wildland Fires. *Environ. Int.* **1991**, *17* (2−3), 117−134.
(24) Kasischke, E. S.; Bruhwiler, L. P. Emissions of Carbon Dioxide, Carbon Monoxide, and Methane from Boreal Forest Fires in 1998. *J. Geophys. Res. Atmospheres* **2002**, *107* (D1), FFR 2-1−FFR 2-14.
(25) Urbanski, S. Wildland Fire Emissions, Carbon, and Climate: Emission Factors. *For. Ecol. Manag.* **2014**, *317*, 51−60.
(26) Holder, A. L.; Ahmed, A.; Vukovich, J. M.; Rao, V. Hazardous Air Pollutant Emissions Estimates from Wildfires in the Wildland Urban Interface. *PNAS Nexus* **2023**, *2* (6), pgad186.
(27) Wang, S.; Bathras, B. L.; Cui, W.; Milazzo, M.; Goldstein, A. H.; Gollner, M. J. Laboratory Quantification of Emissions from Wildland-Urban Interface Fuels Using Fourier-Transform Infrared Spectroscopy. *Environ. Sci. Technol.* **2025**, *59* (25), 12843−12852.
(28) Gurney, K. R.; Patarasuk, R.; Liang, J.; Song, Y.; O'Keeffe, D.; Rao, P.; Whetstone, J. R.; Duren, R. M.; Eldering, A.; Miller, C. The Hestia Fossil Fuel CO2 Emissions Data Product for the Los Angeles Megacity (Hestia-LA). *Earth Syst. Sci. Data* **2019**, *11* (3), 1309−1335.
(29) Eaton Fire Status Update Reports. *CAL Fire*. https://www.fire.ca.gov/incidents/2025/1/7/eaton-fire/updates (accessed 04 15, 2025).
(30) Bruns, E. A.; El Haddad, I.; Slowik, J. G.; Kilic, D.; Klein, F.; Baltensperger, U.; Prévôt, A. S. H. Identification of Significant Precursor Gases of Secondary Organic Aerosols from Residential Wood Combustion. *Sci. Rep.* **2016**, *6* (1), 27881.
(31) Sekimoto, K.; Koss, A. R.; Gilman, J. B.; Selimovic, V.; Coggon, M. M.; Zarzana, K. J.; Yuan, B.; Lerner, B. M.; Brown, S. S.; Warneke, C.; Yokelson, R. J.; Roberts, J. M.; De Gouw, J. High- and Low-Temperature Pyrolysis Profiles Describe Volatile Organic Compound Emissions from Western US Wildfire Fuels. *Atmospheric Chem. Phys.* **2018**, *18* (13), 9263−9281.
(32) Majdi, M.; Sartelet, K.; Lanzafame, G. M.; Couvidat, F.; Kim, Y.; Chrit, M.; Turquety, S. Precursors and Formation of Secondary Organic Aerosols from Wildfires in the Euro-Mediterranean Region. *Atmospheric Chem. Phys.* **2019**, *19* (8), 5543−5569.
(33) Liang, Y.; Weber, R. J.; Misztal, P. K.; Jen, C. N.; Goldstein, A. H. Aging of Volatile Organic Compounds in October 2017 Northern California Wildfire Plumes. *Environ. Sci. Technol.* **2022**, *56* (3), 1557−1567.
(34) Liang, Y.; Stamatis, C.; Fortner, E. C.; Wernis, R. A.; Van Rooy, P.; Majluf, F.; Yacovitch, T. I.; Daube, C.; Herndon, S. C.; Kreisberg, N. M.; Barsanti, K. C.; Goldstein, A. H. Emissions of Organic Compounds from Western US Wildfires and Their Near-Fire Transformations. *Atmospheric Chem. Phys.* **2022**, *22* (15), 9877−9893.
(35) He, Y.; Zhao, B.; Wang, S.; Valorso, R.; Chang, X.; Yin, D.; Feng, B.; Camredon, M.; Aumont, B.; Dearden, A.; Jathar, S. H.; Shrivastava, M.; Jiang, Z.; Cappa, C. D.; Yee, L. D.; Seinfeld, J. H.; Hao, J.; Donahue, N. M. Formation of Secondary Organic Aerosol from Wildfire Emissions Enhanced by Long-Time Ageing. *Nat. Geosci.* **2024**, *17* (2), 124−129.
(36) An Important Update for Customers Near the Eaton Fire—1.10.25 3pm; *SoCalGas*, 2025. https://www.socalgas.com/sites/default/files/2025-01/SCG_1-10-25_Eaton_Fire_Updates.pdf (accessed 05 12, 2025).
(37) Ross, A. N.; Wooster, M. J.; Boesch, H.; Parker, R. First Satellite Measurements of Carbon Dioxide and Methane Emission Ratios in Wildfire Plumes. *Geophys. Res. Lett.* **2013**, *40* (15), 4098−4102.
(38) Akagi, S. K.; Yokelson, R. J.; Wiedinmyer, C.; Alvarado, M. J.; Reid, J. S.; Karl, T.; Crounse, J. D.; Wennberg, P. O. Emission Factors for Open and Domestic Biomass Burning for Use in Atmospheric Models. *Atmospheric Chem. Phys.* **2011**, *11* (9), 4039−4072.
(39) Robinson, C. G.; Wattis, Z. E.; Dooley, C.; Popovic, S. Assessment of the Threat From Wildfires on Above Ground Natural Gas Facilities. In *Volume 2: Pipeline Safety Management Systems; Project Management, Design, Construction, and Environmental Issues; Strain Based Design; Risk and Reliability; Northern Offshore and Production Pipelines. 2018 12th International Pipeline Conference (IPC2018)*; American Society of Mechanical Engineers, 2018; p V002T07A001. DOI: 10.1115/IPC2018-78059.
(40) González, D. J. X.; Morello-Frosch, R.; Liu, Z.; Willis, M. D.; Feng, Y.; McKenzie, L. M.; Steiger, B. B.; Wang, J.; Deziel, N. C.; Casey, J. A. Wildfires Increasingly Threaten Oil and Gas Wells in the Western United States with Disproportionate Impacts on Marginalized Populations. *One Earth* **2024**, *7* (6), 1044−1055.
(41) South Coast AQMD. Mobile Air Monitoring. *2025 Wildfire Response*, 2025. https://www.aqmd.gov/2025-wildfire-response (accessed 05 12, 2025).
(42) Lotrecchiano, N.; Sofia, D.; Giuliano, A.; Barletta, D.; Poletto, M. Pollution Dispersion from a Fire Using a Gaussian Plume Model. *Int. J. Saf. Secur. Eng.* **2020**, *10* (4), 431−439.
(43) Dong, C.; Williams, A. P.; Abatzoglou, J. T.; Lin, K.; Okin, G. S.; Gillespie, T. W.; Long, D.; Lin, Y.-H.; Hall, A.; MacDonald, G. M. The Season for Large Fires in Southern California Is Projected to Lengthen in a Changing Climate. *Commun. Earth Environ.* **2022**, *3* (1), 22.
(44) Vannucci, P. F.; Cohen, R. C. Temperature-Dependent Nighttime Stagnation Episodes Driving Decadal Air Pollutant Exceedances in Los Angeles. *ACS EST Air* **2024**, *1* (6), 474−480.

https://doi.org/10.1021/acsestair.5c00430
ACS EST Air XXXX, XXX, XXX−XXX